Supporting Info

Automated open-source software for charge transport analysis in single-carrier organic semiconductor diodes

Nikolaos Felekidis[1], Armantas Melianas[2] and Martijn Kemerink[1]

[1] Complex Materials and Devices, Department of Physics, Chemistry and Biology, Linköping University, SE-581 83 Linköping, Sweden
[2] Department of Materials Science and Engineering, Stanford University, Stanford, California 94305, USA

Contents

1 - One dimensional drift diffusion model complementary equations

Equation 11 in the main text is solved using the discretization:

$$\frac{1}{h^2}(V_{i+1} + V_{i-1} - 2V_i) = -\frac{\rho_i}{\varepsilon_0 \varepsilon_r} \quad (1)$$

where h is the mesh spacing, V the electrostatic potential, ρ the total charge density, ε_0 the vacuum permittivity and ε_r the dielectric constant. This results in a $N \times N$ tridiagonal matrix $\bar{\bar{P}}$, having on the first and last row only a '1' as entry on the diagonal, to account for the boundary conditions for V as set by the contacts. Using $\bar{\bar{P}}\bar{V} = -\frac{h^2}{\varepsilon_0 \varepsilon_r}\bar{R}$ where $\bar{V}$ is a column vector containing V_i and $\bar{R}$ a column vector containing ρ_i except the first and last entries which are equal to the electrostatic potential of the left and right contact, respectively. Equation 12 in the main text results in hole currents:

$$j_{i+\frac{1}{2}} = -\frac{q\mu_p}{h}(V_{i+1} - V_i)\left(\frac{p_i}{1 - \exp\left(\Delta E_{i+\frac{1}{2}}\right)} + \frac{p_{i+1}}{1 - \exp\left(-\Delta E_{i+\frac{1}{2}}\right)}\right) \quad (2)$$

With, in the normal Scharfetter-Gummel scheme, $\Delta E_{i+\frac{1}{2}} = \frac{V_{i+1} - V_i}{k_B T}$.[1] For brevity, the subscripts in $\mu_{i+\frac{1}{2}}$ are dropped. Note also that the term between brackets is the interpolated hole density $p_{i+1/2}$, i.e. $j_{i+\frac{1}{2}} = -q\mu p_{i+1/2} F_{i+1/2}$ (Ohm's law) where the field $F_{i+1/2} = \frac{V_{i+1} - V_i}{h}$ is constant between mesh points. It should be noted that $p_{i+1/2}$ is not a real density and may be negative in cases diffusion dominates over drift! In order to allow use of the generalized Einstein equation we use $\Delta E_{i+1/2} = \frac{v_{i+1/2} h}{D} = \frac{\mu}{D}(V_{i+1} - V_i)$ as $v = \mu \frac{V_{i+1} - V_i}{h}$ and $D = \mu k_B T$.[2,3] This gives:

$$j_{i+\frac{1}{2}} = -\frac{qD}{h}\left(\frac{\frac{\mu}{D}(V_{i+1} - V_i)p_i}{1 - \exp\left(\frac{\mu}{D}(V_{i+1} - V_i)\right)} + \frac{\frac{\mu}{D}(V_{i+1} - V_i)p_{i+1}}{1 - \exp\left(-\frac{\mu}{D}(V_{i+1} - V_i)\right)}\right) \quad (3)$$

Using the Bernoulli function $B(x) = \frac{x}{1 - \exp(x)} = \frac{x}{2}\left(1 - \frac{1}{\tanh\left(\frac{x}{2}\right)}\right)$ this can be written as

$$j_{i+1/2} = -\frac{qD}{h}\left(B\left(Y_{i+\frac{1}{2}}\right)p_i - B\left(-Y_{i+\frac{1}{2}}\right)p_{i+1}\right) \quad (4)$$

with $Y_{i+1/2} = \frac{\mu}{D}(V_{i+1} - V_i)$. The second guise of the Bernoulli function is preferred for numerical evaluation around $x = 0$. Moreover, using the identity $\frac{x}{\tanh(-x)} = \frac{-x}{\tanh(x)}$, tanh() has to be evaluated only once.

Taking the limit of zero electric field using $B(0) = -1$ it is derived that $j_{i+\frac{1}{2}} = -\frac{qD}{h}(p_{i-1} - p_i)$ which is the common discretization of the diffusion equation for holes, $j_{p,diff} = -qD\frac{\partial p}{\partial x}$. Likewise, taking the limit of dominant drift, $|\mu(V_{i+1} - V_i)| \gg D$, the upwind discretization of the drift equation for holes is obtained, $j_{p,drift} = -q\mu\frac{(V_{i+1} - V_i)}{h}p_{i+1}$ for $(V_{i+1} - V_i) > 0$ and $j_{p,drift} = -q\mu\frac{(V_{i+1} - V_i)}{h}p_i$ for $(V_{i+1} - V_i) < 0$.

For electrons, the current density becomes

$$j_{i+1/2} = -\frac{q\mu}{h}(V_{i+1} - V_i)\left(\frac{n_i}{1-\exp\left(-\Delta E_{i+\frac{1}{2}}\right)} + \frac{n_{i+1}}{1-\exp\left(\Delta E_{i+\frac{1}{2}}\right)}\right) \quad (5)$$

$$j_{i+1/2} = -\frac{qD}{h}\left(\frac{\frac{\mu}{D}(V_{i+1} - V_i)n_i}{1-\exp\left(-\frac{\mu}{D}(V_{i+1} - V_i)\right)} + \frac{\frac{\mu}{D}(V_{i+1} - V_i)n_{i+1}}{1-\exp\left(\frac{\mu}{D}(V_{i+1} - V_i)\right)}\right) \quad (6)$$

$$j_{i+\frac{1}{2}} = -\frac{qD}{h}\left(-B\left(-Y_{i+\frac{1}{2}}\right)n_i + B\left(Y_{i+\frac{1}{2}}\right)n_{i+1}\right) \quad (7)$$

Using the continuity equation in steady state

$$\frac{\partial}{\partial x}j_p = q(G - R) \quad (8)$$

$$\frac{\partial}{\partial x}j_n = -q(G - R) \quad (9)$$

it is derived for holes

$$\frac{j_{i+1/2} - j_{i-1/2}}{h} = q(G_i - R_i) = qU_i \quad (10)$$

and for electrons

$$\frac{j_{i+1/2} - j_{i-1/2}}{h} = -q(G_i - R_i) = -qU_i \quad (11)$$

For equations 11 and 12 above, they can be cast as an $N \times N$ tridiagonal matrix, similarly to the Poisson equation, having only a '1' on the first and last row as entry on the diagonal to account for the boundary conditions for *p* and *n*, respectively, as set by the contacts. For holes one has $\bar{\bar{C}}\bar{P} = qh\bar{U}$ with $\bar{P}$ a column vector containing p_i and $\bar{U}$ a column vector containing U_i except at the 1st and Nth entries that are equal to the densities at the left and right contact, respectively.

2 - Derivation of equation 17 in main text

SCLC zero field mobilities (μ_0) and gamma (γ) values were extracted from the Murgatroyd-Gill law following the equation:[4,5]

$$J = \frac{9}{8}\varepsilon_r\varepsilon_0\mu_0\frac{(V - V_{bi})^2}{L^3}\cdot e^{\left(0.891\gamma\sqrt{\left(\frac{V-V_{bi}}{L}\right)}\right)} \quad (12)$$

where

$$\gamma(T) = \left(\frac{e^3}{\pi\varepsilon\varepsilon_0}\right)^{\frac{1}{2}}\left[\frac{1}{kT}ln\frac{N_c}{N_t} - \frac{1}{(kT)^2}E_{trap}\right] \quad (13)$$

which can be obtained following the derivation by Murgatroyd in Ref. [4] using:

$$J = \frac{9}{8}\mu\epsilon\epsilon_0\frac{V^2}{L^3}\theta_0 e^{\left(\frac{0.891}{kT}\left(\frac{e^3V}{\pi\varepsilon\varepsilon_0 L}\right)^{\frac{1}{2}}\right)} \quad (14)$$

$$\theta_0 = \frac{N_c}{N_t}e^{\left(-\frac{E_{trap}}{kT}\right)} \quad (15)$$

In the above equations ε_0 is the vacuum permittivity, ε_r is the dielectric constant of the material, V is the applied voltage, V_{bi} is the built-in field of the device, μ_0 is the zero field mobility, γ is the field enhancement factor, L is the distance between the electrodes, N_c is the effective density of states, N_t is the density of traps, k is the Boltzmann constant, T is the temperature, e the elementary charge, E_{trap} refers to a single trap situated at energy E_{trap} below the conduction band edge and θ_0 describes the fraction of free charges.

3 - J-V data and SCLC, MG+GDM and DD+eGDM analysis of ternary TQ1:$PC_{71}BM$:$IC_{60}BA$ hole-only devices shown in Figure 3

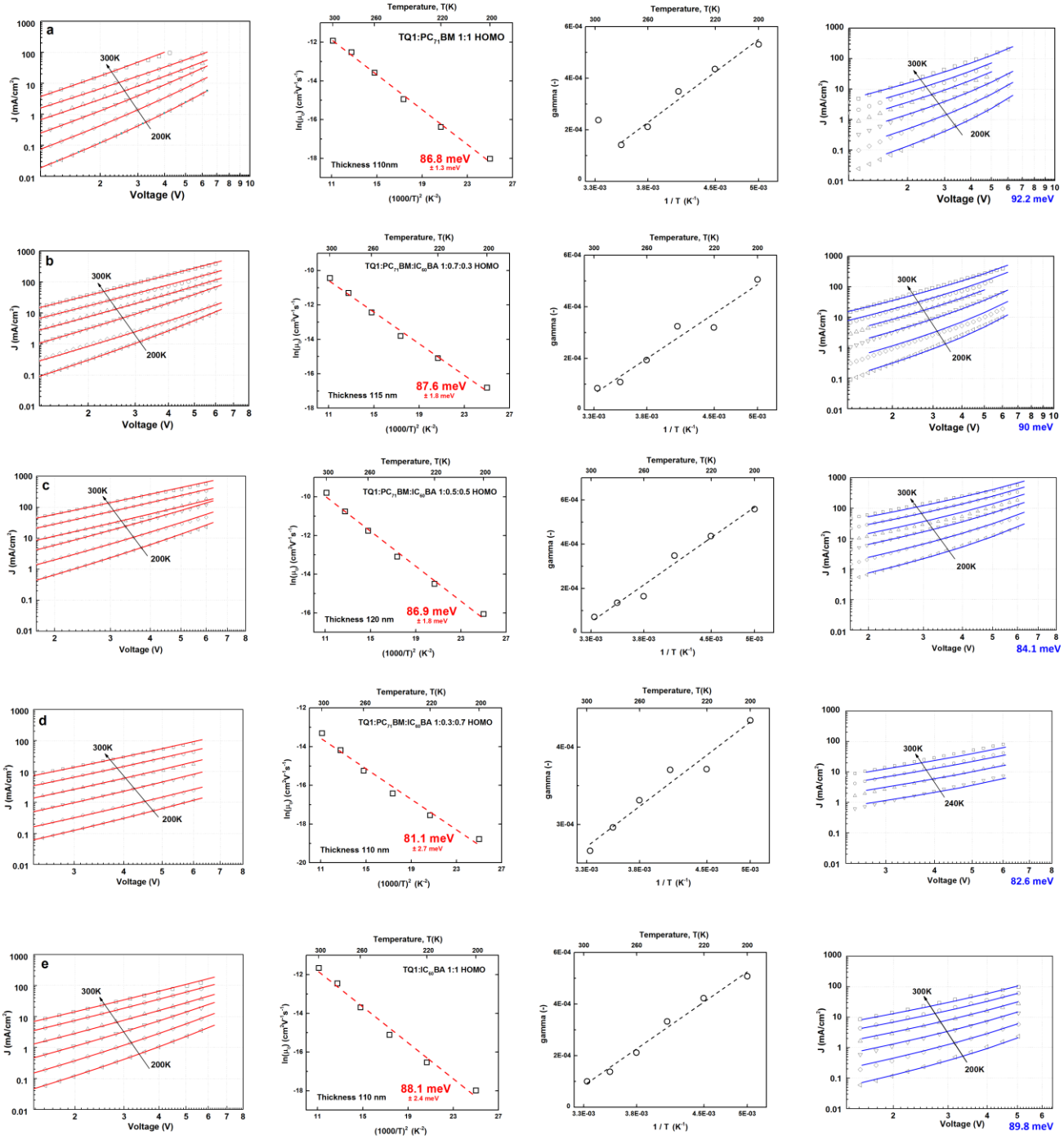

Figure S1. (Left) Hole-only SCLC TQ1:$PC_{71}BM_{1-x}$:$IC_{60}BA_x$ ($0 \leq x \leq 1$) data fitted with the Murgatroyd-Gill law.[4,5](Middle-left) Gaussian disorder model fit and active layer thickness. (Middle-right) Linear fit of the gamma values according to equation 17 in the main text. (Right) SCLC data fitted with the DD+eGDM model.

4 - Gaussian disorder and room temperature zero-field mobilities for MG+GDM and DD+eGDM models of the ternary TQ1:$PC_{71}BM$:$IC_{60}BA$ hole-only devices shown in Figure 3

	MG+GDM		DD+eGDM	
	σ_{HOMO} [meV]	μ_0 (300 K) [$cm^2V^{-1}s^{-1}$]	σ_{HOMO} [meV]	μ_0 (300 K) [$cm^2V^{-1}s^{-1}$]
TQ1:$PC_{71}BM$ 1:1	86.8	$6.62\cdot10^{-6}$	92.2	$6.71\cdot10^{-6}$
TQ1:$PC_{71}BM$:$IC_{60}BA$ 1:0.7:0.3	87.6	$2.92\cdot10^{-5}$	90	$1.87\cdot10^{-5}$
TQ1:$PC_{71}BM$:$IC_{60}BA$ 1:0.5:0.5	86.9	$5.57\cdot10^{-5}$	84.1	$3.2\cdot10^{-5}$
TQ1:$PC_{71}BM$:$IC_{60}BA$ 1:0.3:0.7	81.1	$1.66\cdot10^{-6}$	82.6*	$3.23\cdot10^{-6}$
TQ1:$IC_{60}BA$ 1:1	88.1	$8.66\cdot10^{-6}$	89.8	$5.76\cdot10^{-6}$

Table S1. Gaussian energetic disorder and room temperature zero-field mobilities for TQ1:$PC_{71}BM_{1-x}$:$IC_{60}BA_x$ ($0 \leq x \leq 1$) hole-only devices from the MG+GDM and DD+eGDM models. *The hopping rate and lattice constant were fixed for TQ1:$PC_{71}BM$:$IC_{60}BA$ 1:0.3:0.7 (see Table S3) while 4 temperatures (240K – 300K) were fitted.

All fits were done using the auto-range mode of the SCLC fitting program. The fitting settings for GDM are: nMin=10, Vmin=0.2 V, slope min=1.7, slope target=2, curve min=0, initial guesses: μ^*= 1e-7 $cm^2V^{-1}s^{-1}$ (±3 orders of magnitude), σ=75 meV (limits 25-200 meV), B=$2.8\cdot10^{-5}$(±3 orders of magnitude), T_0=600 K (limits 1-3000 K), $\phi_{1,2}$ = 0.1 (± 0.2 V). The minor difference in Gaussian energetic disorders compared to Ref. [6] is due to the different voltage ranges used for fitting the temperature-dependent JV curves. In Ref. [6] the fitting ranges were set manually and slightly differed among the different JVs while in this case the auto-range mode resulted in a single voltage range for all the JV curves.

For the DD+eGDM model the settings of the fitting program were: nMin=10, Vmin=2 V, slope Min = 1.7, slope target = 2, curve min = -0.5. Initial guesses were: σ=75 meV (± 50 meV), hopping rate 1e9 s^{-1} (±2 orders of magnitude), $\phi_{1,2}$ = 0.1 eV (± 0.2 meV) and a_{NN}=1.2 nm (limits 1 nm – 4 nm). Speed mode was enabled for faster calculations. Thickness was fixed to the experimentally measured value for all material systems. Different initial guess values introduced insignificant variations in the resulting fitting parameters. The rest of the settings were left to the default values.

5 - Fitting parameters of MG+GDM model of Figure 3

	V_{bi} [V]	μ^* [$m^2V^{-1}s^{-1}$]	B [-]	T_0 [K]	Error JV [-]
TQ1:$PC_{71}BM$ 1:1	0.0055	$9.85\cdot10^{-8}$	$1.9\cdot10^{-5}$	379.6	0.00644
TQ1:$PC_{71}BM$:$IC_{60}BA$ 1:0.7:0.3	0.0185	$3.96\cdot10^{-7}$	$2.14\cdot10^{-5}$	328.2	0.00624
TQ1:$PC_{71}BM$:$IC_{60}BA$ 1:0.5:0.5	0.0176	$6.72\cdot10^{-7}$	$2.62\cdot10^{-5}$	318.6	0.00631
TQ1:$PC_{71}BM$:$IC_{60}BA$ 1:0.3:0.7	0.0257	$9.76\cdot10^{-9}$	$8.15\cdot10^{-6}$	2319	0.00955
TQ1:$IC_{60}BA$ 1:1	-0.0320	$1.23\cdot10^{-7}$	$2.23\cdot10^{-5}$	336.2	0.00213

Table S2. Fitting parameters for TQ1:$PC_{71}BM_{1-x}$:$IC_{60}BA_x$ ($0 \le x \le 1$) hole-only devices extracted from the MG+GDM model.

The Error JV is the one returned from the least squares fitting algorithm and refers to the deviation of the fitted curves to all the experimental datasets. The outlying fitting parameters for the TQ1:$PC_{71}BM$:$IC_{60}BA$ 1:0.3:0.7 system originate from the very low measured current densities vs. applied voltage.

6 - Fitting parameters of DD+eGDM model of Figure 3

	Thickness [nm]	ϕ_1 [meV]	ϕ_2 [meV]	Hopping rate [s^{-1}]	Error JV [-]	a_{NN} [nm]
TQ1:$PC_{71}BM$ 1:1	110	100	69	$4.22\cdot10^{9}$	0.02	1.75
TQ1:$PC_{71}BM$:$IC_{60}BA$ 1:0.7:0.3	115	98	80	$9.33\cdot10^{9}$	0.039	1.71
TQ1:$PC_{71}BM$:$IC_{60}BA$ 1:0.5:0.5	120	100	68	$6.15\cdot10^{9}$	0.029	1.93
TQ1:$PC_{71}BM$:$IC_{60}BA$ 1:0.3:0.7	110	160	155	$6\cdot10^{8*}$	0.093	1.8^*
TQ1:$IC_{60}BA$ 1:1	110	99	82	$2.66\cdot10^{9}$	0.019	1.76

Table S3. Simulation parameters from the fitting of TQ1:$PC_{71}BM_{1-x}$:$IC_{60}BA_x$ ($0 \le x \le 1$) hole-only devices with the DD+eGDM model in auto-range mode. *This hopping rate and α_{NN} were fixed as the current density of the TQ1:$PC_{71}BM$:$IC_{60}BA$ 1:0.3:0.7 hole-only devices was low and resulted in high disorder (~125meV) to balance the relatively high hopping rate of $\sim5\cdot10^{9}$.

7 - J-V data and SCLC, MG+GDM-DD+eGDM analysis of pristine and binary hole-only devices used in OPV shown in Figure 4

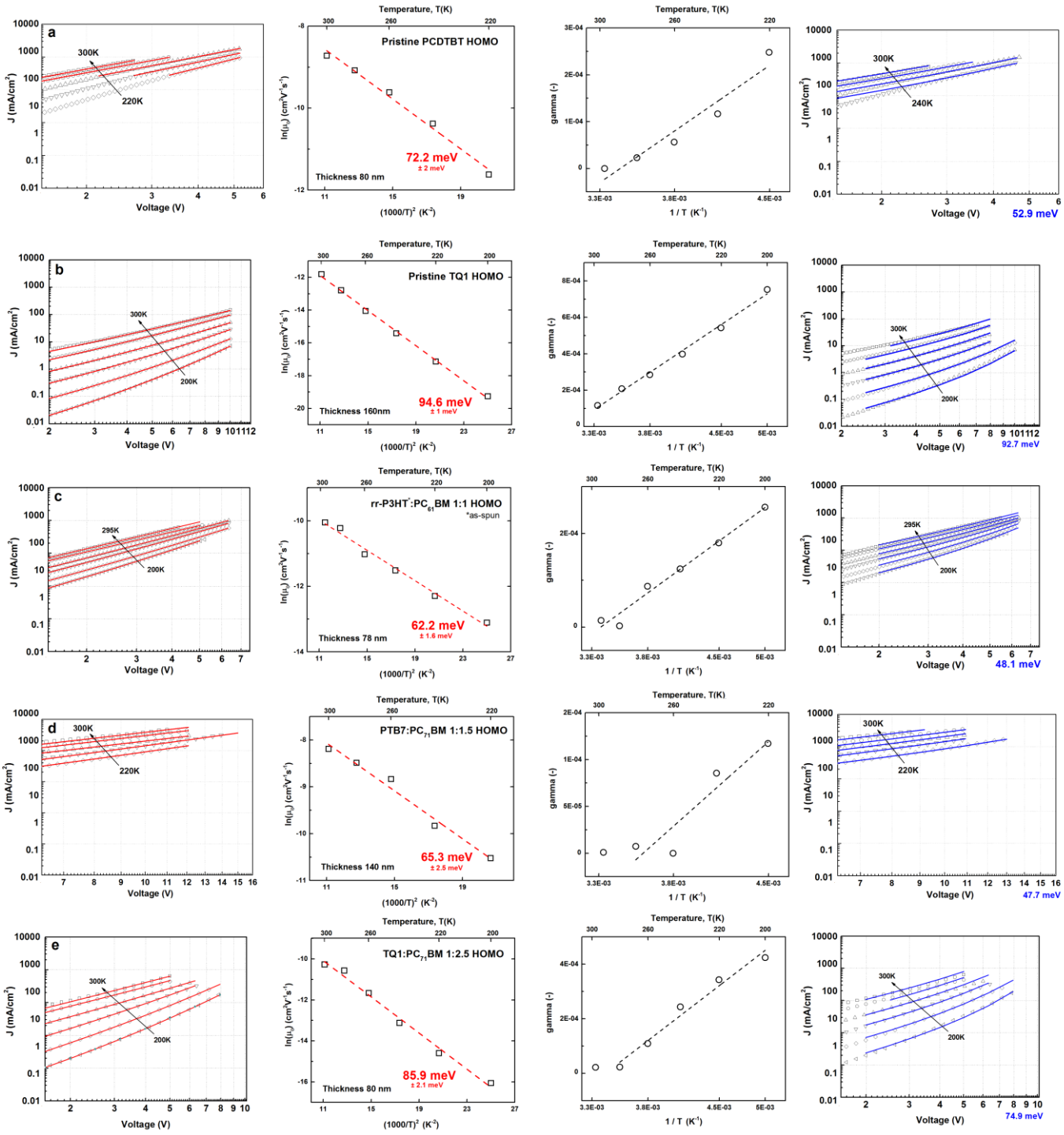

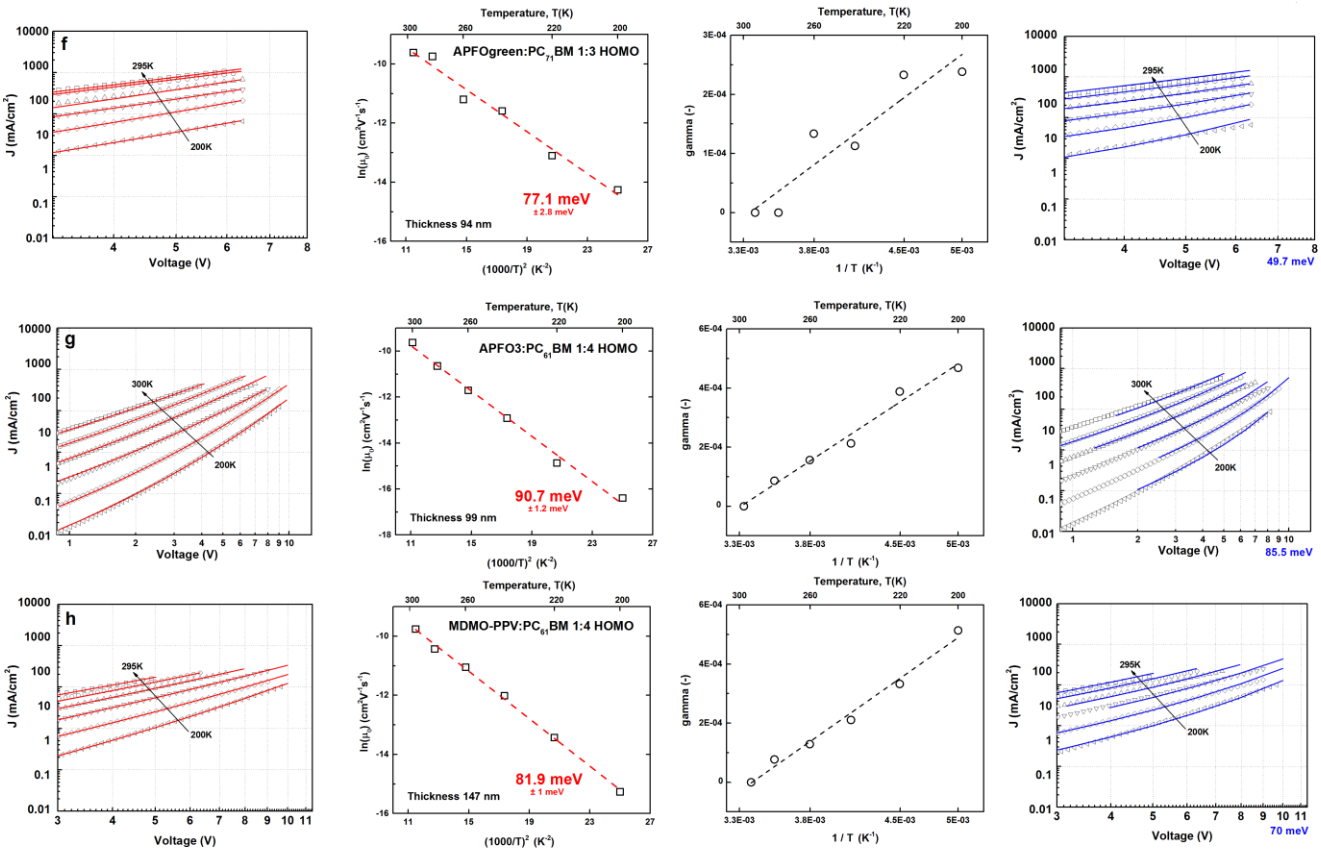

Figure S2. (Left) Hole-only SCLC data fitted with the Murgatroyd-Gill law.[4,5] (Middle-left) Gaussian disorder model fit and active layer thickness. (Middle-right) Linear fit of the gamma values according to equation 17 in the main text. (Right) SCLC data fitted with the Drift Diffusion model.

8 - Gaussian disorder and room temperature zero-field mobilities for MG+GDM and DD+eGDM models of the hole-only devices in Figure 4

	GDM		ODDD	
	σ_{HOMO} [meV]	μ_0 (300 K) [$cm^2V^{-1}s^{-1}$]	σ_{HOMO} [meV]	μ_0 (300 K) [$cm^2V^{-1}s^{-1}$]
PCDTBT pristine	72.2	$1.81 \cdot 10^{-4}$	52.9	$1.01 \cdot 10^{-4}$
TQ1 pristine	94.6	$7.49 \cdot 10^{-6}$	92.7	$5.66 \cdot 10^{-6}$
rrP3HT:PC_{61}BM 1:1	62.2	$4.29 \cdot 10^{-5}$	48.1	$2.46 \cdot 10^{-5}$
TQ1:PC_{71}BM 1:1	86.8	$6.62 \cdot 10^{-6}$	92.2	$6.71 \cdot 10^{-6}$
TQ1:IC_{60}BA 1:1	88.1	$8.66 \cdot 10^{-6}$	89.8	$5.76 \cdot 10^{-6}$
PTB7:PC_{71}BM 1:1.5	65.3	$2.78 \cdot 10^{-4}$	47.7	$2.86 \cdot 10^{-4}$
TQ1:PC_{71}BM 1:2.5	85.9	$3.48 \cdot 10^{-5}$	74.9	$2.27 \cdot 10^{-5}$
APFOGreen:PC_{71}BM 1:3	77.1	$6.69 \cdot 10^{-5}$	49.7	$7.93 \cdot 10^{-5}$
APFO3:PC_{61}BM 1:4	90.7	$6.59 \cdot 10^{-5}$	85.5	$4.12 \cdot 10^{-5}$
MDMO_PPV:PC_{61}BM 1:4	81.9	$5.78 \cdot 10^{-5}$	70	$4.27 \cdot 10^{-5}$

Table S4. Gaussian energetic disorder and room temperature zero-field mobilities from the MG+GDM and DD+eGDM models for pure and binary hole-only devices of Figure 4.

The settings and initial parameter values are the same as in section 4 in the SI.

9 - Fitting parameters of MG+GDM model of Figure 3

	Vbi [V]	**μ^*** [$m^2V^{-1}s^{-1}$]	**B** [-]	**T_0** [K]	**Error JV** [-]
PCDTBT pristine	0.19	$7.32\cdot10^{-7}$	$2.11\cdot10^{-5}$	268.3	0.0071
TQ1 pristine	-0.199	$2.48\cdot10^{-7}$	$3.16\cdot10^{-5}$	324.2	0.002
rrP3HT:PC_{61}BM 1:1	0.0113	$5.9\cdot10^{-8}$	$1.44\cdot10^{-5}$	290.3	$2.1\cdot10^{-5}$
TQ1:PC_{71}BM 1:1	0.0055	$9.85\cdot10^{-8}$	$1.9\cdot10^{-5}$	379.6	0.00644
TQ1:IC_{60}BA 1:1	-0.0320	$1.23\cdot10^{-7}$	$2.23\cdot10^{-5}$	336.2	0.00213
PTB7:PC_{71}BM 1:1.5	-0.199	$5.22\cdot10^{-7}$	$1.42\cdot10^{-5}$	264.7	$8.7\cdot10^{-4}$
TQ1:PC_{71}BM 1:2.5	-0.077	$5.35\cdot10^{-7}$	$2.5\cdot10^{-5}$	283.8	$2.9\cdot10^{-4}$
APFOGreen:PC_{71}BM 1:3	-0.199	$3.93\cdot10^{-7}$	$1.39\cdot10^{-5}$	298.6	0.0019
APFO3:PC_{61}BM 1:4	-0.19	$1.27\cdot10^{-6}$	$2.45\cdot10^{-5}$	302.1	0.0012
MDMO_PPV:PC_{61}BM 1:4	-0.139	$5.71\cdot10^{-7}$	$2.64\cdot10^{-5}$	293.9	0.0019

Table S5. Fitting parameters for pristine, binary and ternary hole-only devices of Figure 4 extracted from the MG+GDM model in auto-range mode.

For the material systems TQ1 pristine, PTB7:PC_{71}BM 1:1.5, APFOGreen:PC_{71}BM 1:3 and APFO3:PC_{61}BM 1:4 the V_{bi} was ~0.4V when the fitting margins were set to 'infinity'. However, the improvement on the JV fits and the difference in the mobilities and energetic disorder were negligible.

10 - Fitting parameters of DD+eGDM model of Figure 4

	Thickness [nm]	**ϕ1** [meV]	**ϕ2** [meV]	**Hopping rate** [s^{-1}]	**Error JV** [-]	**a_{NN}** [nm]
PCDTBT pristine	80	168	123	$1.12\cdot10^{9}$	0.001	1.66
TQ1 pristine	160	127	57	$3.12\cdot10^{9}$	0.068	1.93
rrP3HT:PC_{61}BM 1:1	78	111	85.7	$2\cdot10^{8}$	0.01	1.59
TQ1:PC_{71}BM 1:1	110	100	69	$4.22\cdot10^{9}$	0.02	1.75
TQ1:IC_{60}BA 1:1	110	99	82	$2.66\cdot10^{9}$	0.019	1.76
PTB7:PC_{71}BM 1:1.5	140	30	148	$2\cdot10^{9}$	0.004	1.3
TQ1:PC_{71}BM 1:2.5	80	101	105	$3.37\cdot10^{9}$	0.028	1.31
APFOGreen:PC_{71}BM 1:3	94	196	158	$3.58\cdot10^{8}$	0.03	2.28
APFO3:PC_{61}BM 1:4	99	134	53.7	$2.06\cdot10^{10}$	0.02	1.3
MDMO_PPV:PC_{61}BM 1:4	147	103	96.9	$1.8\cdot10^{9}$	0.04	1.9

Table S6. Fitting parameters for pristine, binary and ternary hole-only devices of Figure 4 extracted from the DD+eGDM model in auto-range mode. The simulations were run with the same settings and initial guesses as in section 5.

11 – DD + eGDM, cGDM and ET-GDM comparison

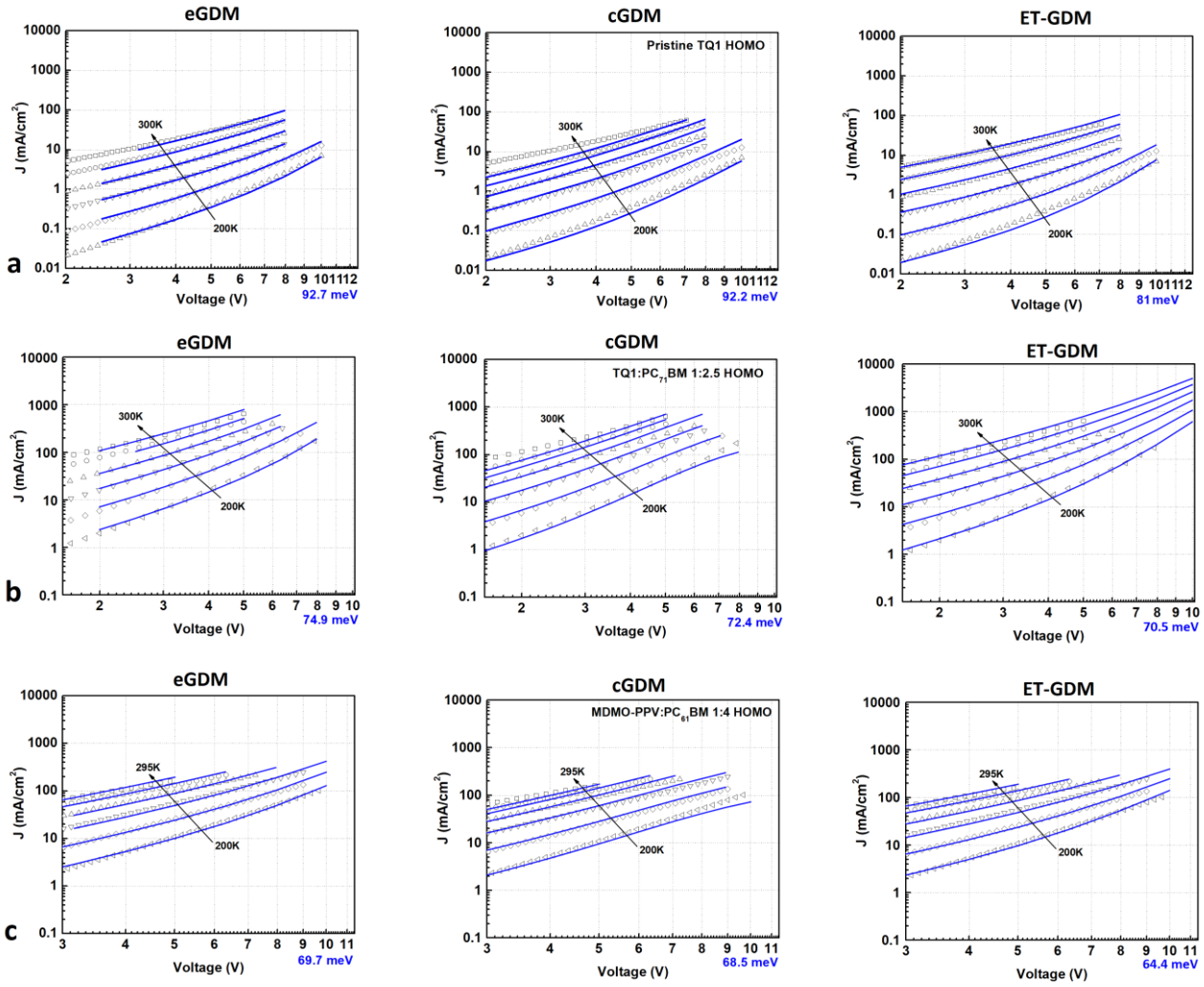

Figure S3. SCLC fits and extracted Gaussian disorder (in blue) for DD+eGDM, cGDM and ET-GDM for a) pristine TQ1 b) TQ1:$PC_{71}BM$ 1:2.5 and c) MDMO-PPV:$PC_{61}BM$ 1:4

12 – DD+ET-GDM fitting parameters

	v_0 [s^{-1}]	Error JV [-]	a_{NN} [nm]	σ [meV]	α [nm]
PCDTBT pristine	$1.025 \cdot 10^9$	0.028	1.94	61.6	0.22
TQ1 pristine	$1.074 \cdot 10^9$	0.067	1.10	81	0.32
TQ1:PC_{71}BM 1:1	$1.1 \cdot 10^9$	0.03	1.18	81.3	0.3
TQ1:PC_{71}BM:IC_{60}BA 1:0.7:0.3	$1.27 \cdot 10^9$	0.04	1.75	82	0.26
TQ1:PC_{71}BM:IC_{60}BA 1:0.5:0.5	$1.64 \cdot 10^9$	0.03	1.47	75.2	0.34
TQ1:PC_{71}BM:IC_{60}BA 1:0.3:0.7	$1.1 \cdot 10^9$	0.129	1.1	89.6	0.31
TQ1:IC_{60}BA 1:1	$1 \cdot 10^9$	0.03	1	78.9	0.3
rrP3HT:PC_{61}BM 1:1	$1 \cdot 10^9$	0.9	1	57.3*	0.27
PTB7:PC_{71}BM 1:1.5	$2.2 \cdot 10^9$	0.002	1.45	53.1	0.13
TQ1:PC_{71}BM 1:2.5	$1.02 \cdot 10^9$	0.02	1.26	70.2	0.20
APFOGreen:PC_{71}BM 1:3	$2 \cdot 10^9$	0.03	1.36	68.3	0.19
APFO3:PC_{61}BM 1:4	$1.7 \cdot 10^9$	0.019	2.05	82.3	0.18
MDMO_PPV:PC_{61}BM 1:4	$1.41 \cdot 10^9$	0.04	1.21	64.4	0.33

Table S7. Extracted parameters from fitting the temperature dependent SCLC data with the DD+ET-GDM model for all material systems. *The model could not accurately fit the data for rrP3HT:PC_{61}BM 1:1

13 - Arrhenius analysis for μ^*=10 $cm^2V^{-1}s^{-1}$

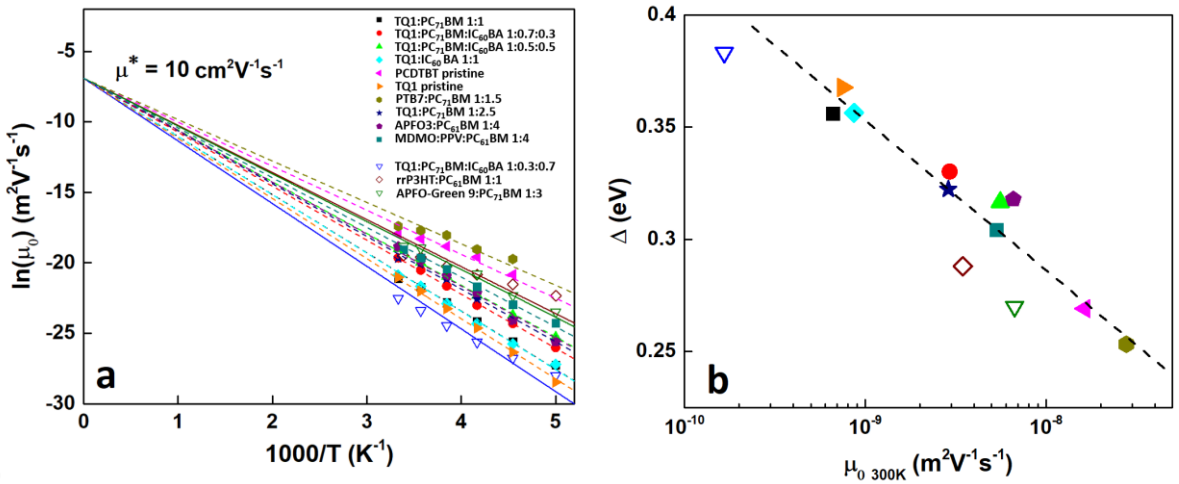

Figure S4. a) Zero-field mobilities for hole-only pristine, binary and ternary material systems fitted with equation 17 in the main text with Δ as a free parameter and a fixed μ^*=10 $cm^2V^{-1}s^{-1}$. The plot is scaled as in Ref. [7] showing a 'universal' μ^* at infinite temperature. Open symbols with solid line fits indicate the material systems that do not show strong correlation between Δ and zero field mobility at 300 K b) Resulting Δ values versus zero field mobilities at 300 K for all material systems investigated in this work. The dashed line is a guide to the eye. Stronger correlation (10 out of 13 material systems, indicated with solid symbols) is noticed when μ^* is set equal to 10 $cm^2V^{-1}s^{-1}$ compared to μ^* set as a free parameter (c.f. Figure 5 and discussion in the main text).

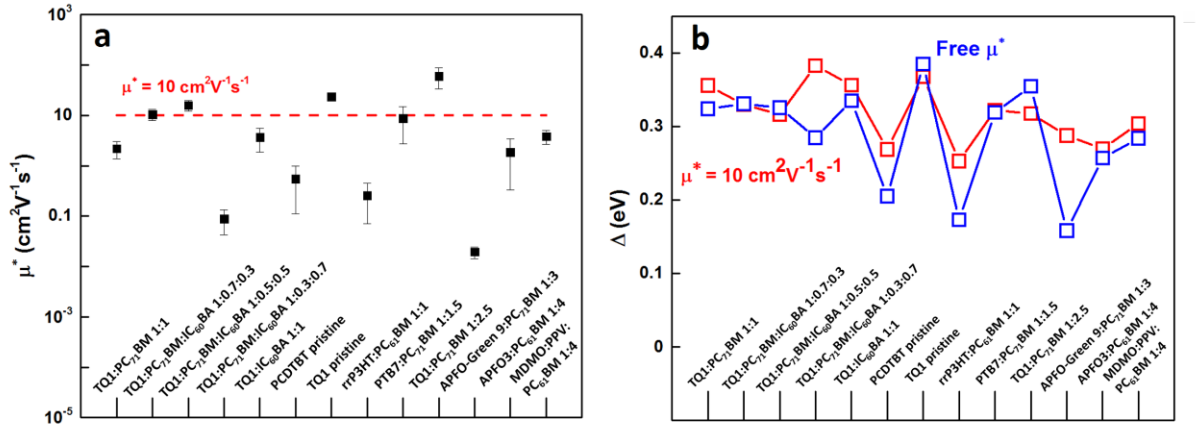

Figure S5. a) Zero-field mobilities at infinite temperature for hole-only pristine, binary and ternary material systems fitted with equation 17 in the main text with μ^* and Δ set as free parameters (black squares). The red dashed line is the fixed μ^*=10 $cm^2V^{-1}s^{-1}$. b) Activation energies Δ for free μ^*(blue traces) and fixed μ^*=10 $cm^2V^{-1}s^{-1}$ (red traces).

	Free μ^* [$cm^2V^{-1}s^{-1}$]	**Δ** [eV]	**Δ** μ^*=10 $cm^2V^{-1}s^{-1}$ [meV]
TQ1:PC_{71}BM 1:1	2.18	0.32	0.35
TQ1:PC_{71}BM:IC_{60}BA 1:0.7:0.3	10.49	0.33	0.33
TQ1:PC_{71}BM:IC_{60}BA 1:0.5:0.5	15.75	0.32	0.31
TQ1:PC_{71}BM:IC_{60}BA 1:0.3:0.7	0.08	0.28	0.38
TQ1:IC_{60}BA 1:1	3.66	0.33	0.35
PCDTBT pristine	0.54	0.20	0.26
TQ1 pristine	23.34	0.38	0.36
rrP3HT:PC_{61}BM 1:1	0.019	0.15	0.28
PTB7:PC_{71}BM 1:1.5	0.25	0.17	0.25
TQ1:PC_{71}BM 1:2.5	8.76	0.31	0.32
APFOGreen:PC_{71}BM 1:3	1.86	0.25	0.26
APFO3:PC_{61}BM 1:4	60.16	0.35	0.31
MDMO_PPV:PC_{61}BM 1:4	3.82	0.28	0.3

Table S8. Fitting parameters from Arrhenius-type analysis of all material systems with equation 17 in the main text for free and constrained μ^*(show in Figures S3,S4).

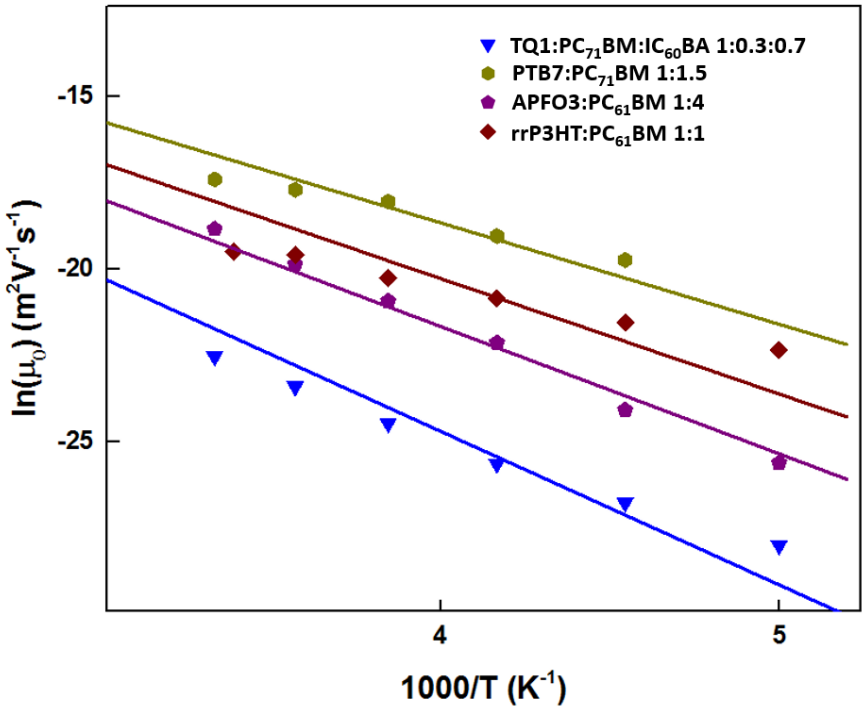

Figure S6. Zoomed-in view of zero-field mobilities for hole-only devices fitted with equation 17 using a fixed μ^*=10 $cm^2V^{-1}s^{-1}$ while the activation energy Δ is set as a free fitting parameter. The universal μ^* does not result in good fits for TQ1:PC_{71}BM:IC_{60}BA 1:0.3:0.7, PTB7:PC_{71}BM 1:1.5, APFO3:PC_{61}BM 1:4 and rrP3HT:PC_{61}BM 1:1 hole-only devices.

14 - Forced γ=0 mobility and disorder analysis for APFO3:PC_{61}BM 1:4

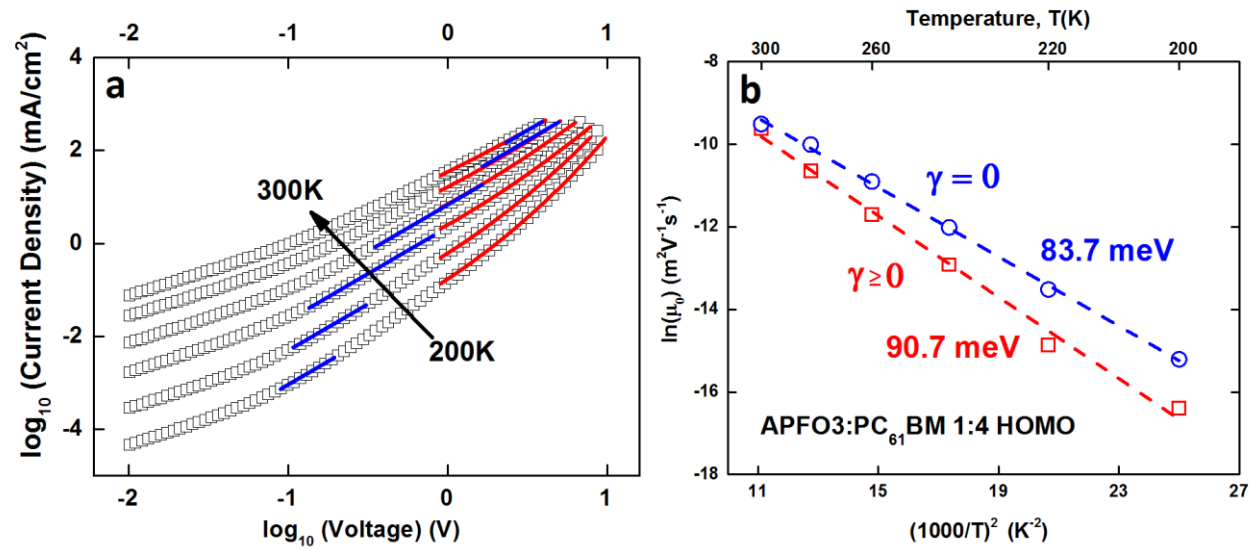

Figure S7. a) Temperature-dependent SCLC data for APFO3:PC_{61}BM 1:4 hole-only devices (black open symbols) fitted with Eq. 17 using γ ≥ 0 (red lines) and γ = 0 (blue lines); b) Extracted zero-field mobilities vs $1/T^2$ for γ ≥ 0 (red open squares) and γ = 0 (blue open circles).

15 - Material Abbreviations

TQ1 = poly[[2,3-bis(3-octyloxyphenyl)-5,8-quinoxalinediyl]-2,5-thiophenediyl]
$PC_{71}BM$ = [6,6]-phenyl C71 butyric acid methyl ester
$PC_{61}BM$ = [6,6]-phenyl C61 butyric acid methyl ester
$IC_{60}BA$ = 1',1'',4',4''-tetrahydro-di[1,4]methanonaphthaleno-[1,2:2',3',56,60:2',3''][5,6]fullerene-C60
PTB7 = poly({4,8-bis[(2-ethylhexyl)oxy]benzo[1,2-b:4,5-b']-dithiophene-2,6-diyl}{3-fluoro-2-[(2-ethylhexyl)carbonyl]-thieno[3,4-b]thiophenediyl})
P3HT = poly(3-hexylthiophene-2,5-diyl)
PCDTBT = poly[N-9'-heptadecanyl-2,7-carbazole-alt-5,5-(4',7'-di-2-thienyl-2',1',3'-benzothiadiazole)], poly[[9-(1-octylnonyl)-9H-carbazole-2,7-diyl]-2,5-thiophenediyl-2,1,3-benzothiadiazole-4,7-diyl-2,5-thiophenediyl]
MDMO PPV = poly[2-methoxy-5-(3',7'-dimethyloctyloxy)-1,4-phenylenevinylene]
APFO3 = poly[(9,9-dioctylfluorenyl-2,7-diyl)-alt-5,5-(40,70-di-2-thienyl-20,10,30-benzothiadiazole)]

16 – Fabrication parameters

	c [g/L]	**solvent**	**Spin coating speed** [rpm / sec]
PCDTBT pristine	25	ODCB	500 / 120
TQ1 pristine	25	ODCB	500 / 60
TQ1:$PC_{71}BM$ 1:1	25	ODCB	500 / 60
TQ1:$PC_{71}BM$:$IC_{60}BA$ 1:0.7:0.3	25	ODCB	500 / 60
TQ1:$PC_{71}BM$:$IC_{60}BA$ 1:0.5:0.5	25	ODCB	500 / 60
TQ1:$PC_{71}BM$:$IC_{60}BA$ 1:0.3:0.7	25	ODCB	500 / 60
TQ1:$IC_{60}BA$ 1:1	25	ODCB	500 / 60
rrP3HT:$PC_{61}BM$ 1:1	20	CB	1000 / 60
PTB7:$PC_{71}BM$ 1:1.5	20	ODCB	500 / 60
TQ1:$PC_{71}BM$ 1:2.5	25	ODCB	500 / 60
APFOGreen:$PC_{71}BM$ 1:3	15	CF	1500 / 60
APFO3:$PC_{61}BM$ 1:4	20	CF	1500 / 60
MDMO_PPV:$PC_{61}BM$ 1:4	20	CB	500 / 60

Table S9. Solvent, active layer concentration and spin coating speed parameters for all material systems

None of the material systems was annealed or blended with any additives. After the first spin coating step (indicated in the table) all samples were dried with a second spin coating step of 3000 rpm for 60 seconds.

17 - References

[1] D.L. Scharfetter, H.K. Gummel, Large-signal analysis of a silicon Read diode oscillator, IEEE Trans. Electron Devices. 16 (1969) 64–77. doi:10.1109/T-ED.1969.16566.

[2] C. Pflumm, Simulation homogener Barrierenentladungen inklusive der Elektrodenbereiche, Tenea, 2004.

[3] W.R. Frensley, Scharfetter-Gummel Discretization Scheme for Drift-Diffusion Equations, Numer. Simul. Optoelectron. Devices NUSOD. (2004). doi:10.1109/NUSOD.2012.6316560.

[4] P.N. Murgatroyd, Theory of space-charge-limited current enhanced by Frenkel effect, J. Phys. Appl. Phys. 3 (1970) 308. doi:10.1088/0022-3727/3/2/308.

[5] W.D. Gill, Drift mobilities in amorphous charge-transfer complexes of trinitrofluorenone and poly-n-vinylcarbazole, J. Appl. Phys. 43 (1972) 5033–5040. doi:10.1063/1.1661065.

[6] N. Felekidis, A. Melianas, M. Kemerink, Design Rule for Improved Open-Circuit Voltage in Binary and Ternary Organic Solar Cells, ACS Appl. Mater. Interfaces. 9 (2017). doi:10.1021/acsami.7b08276.

[7] N.I. Craciun, J. Wildeman, P.W.M. Blom, Universal Arrhenius Temperature Activated Charge Transport in Diodes from Disordered Organic Semiconductors, (n.d.). doi:10.1103/PhysRevLett.100.056601.